ORIGINAL PAPER

Performance evaluation of Si/Fe$_3$O$_4$ nanoparticles in water-based mud in presence of different Mg^{2+}, K$^+$, Na$^+$ salts: experimental and stability visualization study

Shaine Mohammadali Lalji[1] · Syed Imran Ali[1] · Zeeshan Ali Lashari[2] · Suresh Kumar Panjwani[2] · Muneeb Burney[3]

Abstract

The revolutionized field of nanotechnology emerged in the oil and gas sector to enhance drilling fluid performance. This technology increases the success rate of drilling operations in different environments. However, their performance in presence of various salts has not been entirely discovered up till now. In this research, three different salt mud systems that include KCl, NaCl and MgCl$_2$ were prepared and coated with silica iron oxide nanoparticles. The rheological and filtration characteristics of all the samples with the joint interaction of salt and nanoparticles were analyzed. Additionally, the stability of the mud samples after the interaction between the two entities was investigated using a visualization tool. This unique application will be useful in observing the changes in the mud system during nonproductive time events (NPT). The result of the study reveals that all the fluids in the presence of these entities showed shear thinning behavior with flow index < 1. Reduction in shear stresses in the salt systems was observed mainly because of the neutralization of the negative charges associated with the base mud system. However, this behavior was weaker in monovalent cations as compared with divalent. KCL/(Si/Fe$_3$O$_4$) demonstrates the most stable mud system when investigated through intensity profile plots. Minimum segregation and maximum dispersion were the key parameters that demonstrated its stability. Moreover, all three cations in the presence of Si/Fe$_3$O$_4$ nanoparticles reduce the filtrate loss volume and provide a thin and smooth mud cake. The Si/Fe$_3$O$_4$ because of its spherical bead shape plugs the pore spacing of the filter paper while blocking of microsize spacing was done with the help of cations.

Keywords Filtration behavior · Image processing technique · Intensity profile plots · Rheological properties

Abbreviations

WBDFs	Water-based drilling fluids
OBDFs	Oil-based drilling fluids
PAC	Polyanionic cellulose
NPs	Nanoparticles
PV	Plastic viscosity
YP	Yield point
AV	Apparent viscosity
GS	Gel strength
g	Grams
cc	Centimeter cube
K$^+$	Potassium ion
Na$^+$	Sodium ion
Mg^{2+}	Magnesium ion
cP	Centipoise
ppg	Pound per gallon

✉ Syed Imran Ali
engrimran@neduet.edu.pk

Shaine Mohammadali Lalji
shaine@neduet.edu.pk

Zeeshan Ali Lashari
zalashari@duet.edu.pk

Suresh Kumar Panjwani
suresh.panjwani@duet.edu.pk

Muneeb Burney
muneeb.burney@molpakistan.com

1   Department of Petroleum Engineering, NED University of Engineering and Technology, Karachi, Pakistan

2   Department of Petroleum and Gas Engineering, Dawood University of Engineering and Technology, Karachi, Pakistan

3   MOL Pakistan Oil and Gas Company Ltd. B.V., Islamabad, Pakistan

∑ Springer

Introduction

Drilling fluids are an integral part of any drilling operation as they provide multiple functions during their circulation in the wellbore (Tahr et al. 2023). The success of a drilling operation is primarily dependent on the performance of the drilling fluid system as it can account for more than 15–18% of the entire cost of the well (Mohamed et al. 2010; Yalman et al. 2022). An efficient drilling fluid serves in removing the drill cuttings from the wellbore, maintaining a hydrostatic pressure across the exposed formations, cooling and lubricating the drilling bits, maintaining a stable borehole and minimizing the damage across the pay zone (Tahr et al. 2023; Sajjadian et al. 2020).

Drilling fluids are classified into four major categories (Xie et al. 2018; Jiang et al. 2022; Karakosta et al. 2021; Zhao et al. 2022; Medved et al. 2022; Lalji et al. 2022b): (1) water-based drilling fluids (WBDFs), (2) oil-based drilling fluids (OBDFs), (3) synthetic-based drilling fluids (SBDFs) and (4) pneumatic drilling fluid (air, mist, foam and gas). The selection of a drilling fluid is based generally on four major factors that include technical performance, safety, economy and environmental awareness (Ismail et al. 2017; Tahr et al. 2023). Even though OBDFs have proved to be more efficient as compared to WBDFs, especially in maintaining the stability of the borehole and in preventing damage to the formation, their use has been minimized about to being costly as well as being hazardous to the environment (Tahr et al. 2023). Hence, WBDFs have become a more common type of drilling fluid used in oil and gas exploration around the globe (Tahr et al. 2023). The use of WBDFs has several challenges attached to it such as a reduction of penetration rate, pressure losses due to an increase in friction in the drill string as well as wellbore instability issues (Tahr et al. 2023). To encounter these challenges, researchers have been studying the role of different additives both conventional as well as unconventional (biodegradable waste and nanomaterials) in improving the performance of the WBDFs.

A simple WBDF is basically a combination aqueous phase of water with clay and some other additives (Mohamed et al. 2010). The nature and amount of these additives depend upon the performance and the unique capabilities required for a successful and safe drilling operation. Various additives are used for the preparation of drilling fluids that depend upon the usage function including controlling viscosity, building gel strength, inhibiting shale swelling, controlling filtration loss and loss circulation (Tahr et al. 2023; Awele 2014; Alyasiri et al. 2017). Initially, it all starts with bentonite, a clay mineral in nature belonging to the montmorillonite group. This is generally utilized in WBDFs as a shear thinning viscosifiers and for the creation of a thin and low permeability filter cake along the exposed formation while drilling (Vryzas et al. 2016). Nevertheless, a significant drawback related to bentonite particles lies in their negatively charged surface (Martin et al. 2023). This characteristic along with the pH of the aqueous medium affects the stability of the colloidal system (Martin et al. 2023). These properties enable bentonite to create flocculation and aggregation, which eventually impacts the rheological and filtration behavior of the mud (Martin et al. 2023). Next were the polymers such as xanthan gum, polyacrylamide and carboxymethylcellulose that were commonly used in WBDFs to improve the viscosity as well as the filtrate loss property of the drilling fluid (Ahmad et al. 2018; Hamed and Belhadri 2009; Hermoso et al. 2014; Ma et al. 2018; Nmegbu 2014; Xie et al. 2018). Additionally polymers such as lignosulphonates and polyanionic cellulose (PAC) are also commonly used to improve the rheological properties such as plastic viscosity, yield point and gelling behavior of the drilling fluids (Zhang et al. 2012).

Table 1 Materials used in the current study and their properties

Material	Source	Properties
Ethanol	Local vendor	
Tetraethyl orthosilicate (TEOS)		Preparation of nanoparticles
Neodymium magnet		Used to separate NPs from mixture
Ammonia		Used to maintain pH of the solution
pH meter		Check pH of the solution
Tap water	Directly from tap	Acts as continuous phase in the preparation of drilling fluid
Soda ash	Service company	Used to prevent contamination of tap water
Salts		Improves rheological features of mud
Xanthan gum		Viscosifiers
Barite		Weighting material
PAC		Viscosifiers

Fig. 1 Flowchart demonstrating the process for the synthesis of Si/Fe$_3$O$_4$ nanoparticles

Shales are the most common formation encountered during any drilling activity. Severe wellbore integrity issues arise upon its contact with water-based mud systems. For this monovalent and divalent cationic salts such as NaCl, KCl and MgCl$_2$ are commonly used to minimize shale swelling behavior during drilling activity (Kuma et al. 2020). Swelling of shale is generally considered to be the result of penetration of water molecules into the lattice like structure of the clay minerals in shale. The monovalent and divalent ions present in these salts inhibit shale formation from swelling by entering the lattice of the drilling mud or formation instead of the water ions (Kuma et al. 2020). The limitation of polymeric material at elevated temperatures and the toxicity along with sedimentation problems in salt muds demand another solution to tackle this formation. Therefore, the revolutionized field of nanotechnology emerged in the oil and gas sector.

Worldwide, extensive research has been carried out in the field of nanofluids (nano-based WBDFs). These nanofluids have shown great potential in increasing the rheological properties, such as apparent viscosity, plastic viscosity and gel strength (Özkan et al. 2020; Minakov et al. 2018), improving filtration control (Minakov et al. 2018) as well as shale inhibition property of the drilling fluid (Sangwai 2020). Ali et al. (2022) studied the effect of employing SiO$_2$ and TiO$_2$ NPs on the rheological properties of WBDFs and found a significant improvement in the thinning behavior of the drilling fluid. Al-Saba et al. (2018) reported improvement in the rheological properties of the WBDF as he compared three different types of nanomaterials (MgO, CuO and Al$_2$O$_3$) at different sizes (20–40 nm) and concentrations (0.5–1.5 wt.%). Afolabi et al. (2018) were able to reduce the amount of filtrate loss by 25% when they used silica NPs as an additive in WBDF. Mao et al. (2015) and Javeri et al. (2011) also studied the effect of using silicon dioxide NPs in WBDFs and found significant improvement in fluid loss as well as thickness of filter cake. Vryzas et al. (2016) used Fe$_3$O$_4$ NPs at (6–8 nm size and 0.5% concentration) and found that the fluid loss was reduced from 17.5 to 10.5 mL whereas the filter cake thickness also improved from 7 to 9 mm. Rezaei et al. (2020) used a combination of Fe$_3$O$_4$ NPs and different cationic salts to improve the rheological and filtration characteristics of WBDFs. Apart from all the improvements in the characteristics of the mud system, there are severe limitations/constraints present with the use of nanoparticles, which impacts the cutting transportation mechanism (Ghasemi 2018). When a negatively charged nanodimension material interacts with an additive consisting of a negatively charged surface, an increase in repulsive forces is experienced. These repelling forces create deflocculation that ultimately lowers the cutting carrying capacity and increases the viscosity of the mud during drilling activity (Martin et al. 2023).

The study in this research aims the rheological and filtration characteristics of WBDFs in the presence of different cations and silica-coated iron oxide nanoparticles. It can be noted that for the first time this type of nanomaterial is employed as an additive in drilling fluid. Moreover, to the best of our knowledge, no such interaction has been recorded up till now. Salts are added as a primary inhibitor for shale swelling. Moreover, they can dephase any drilling mud by entering into the system through different sources. Therefore, it is extremely important to examine the variation in the performance of WBDF in the presence of different cationic salts. Hence, it is the focus of the study to explore the effect on the rheological and filtration properties of WBDF in the existence of both salt and NPs. In this work, the rheological performance of three salts including KCl, NaCl and MgCl$_2$ is evaluated in the presence of silica-coated iron oxide nanoparticles. The study is similar to Rezaei et al. (2020); however, iron oxide nanoparticles are modified and coated with silica. Moreover, the investigation in this research employs the most common salts (KCl, NaCl and MgCl$_2$) of the oil and gas sector. In addition, for the first time, a novel application of image processing technique is used to monitor the stability of each mud sample. This novel method will help

Fig. 2 Characterization of silica-coated Si/Fe$_3$O$_4$. **a** XRD analysis, **b** FTIR, **c** SEM imaging
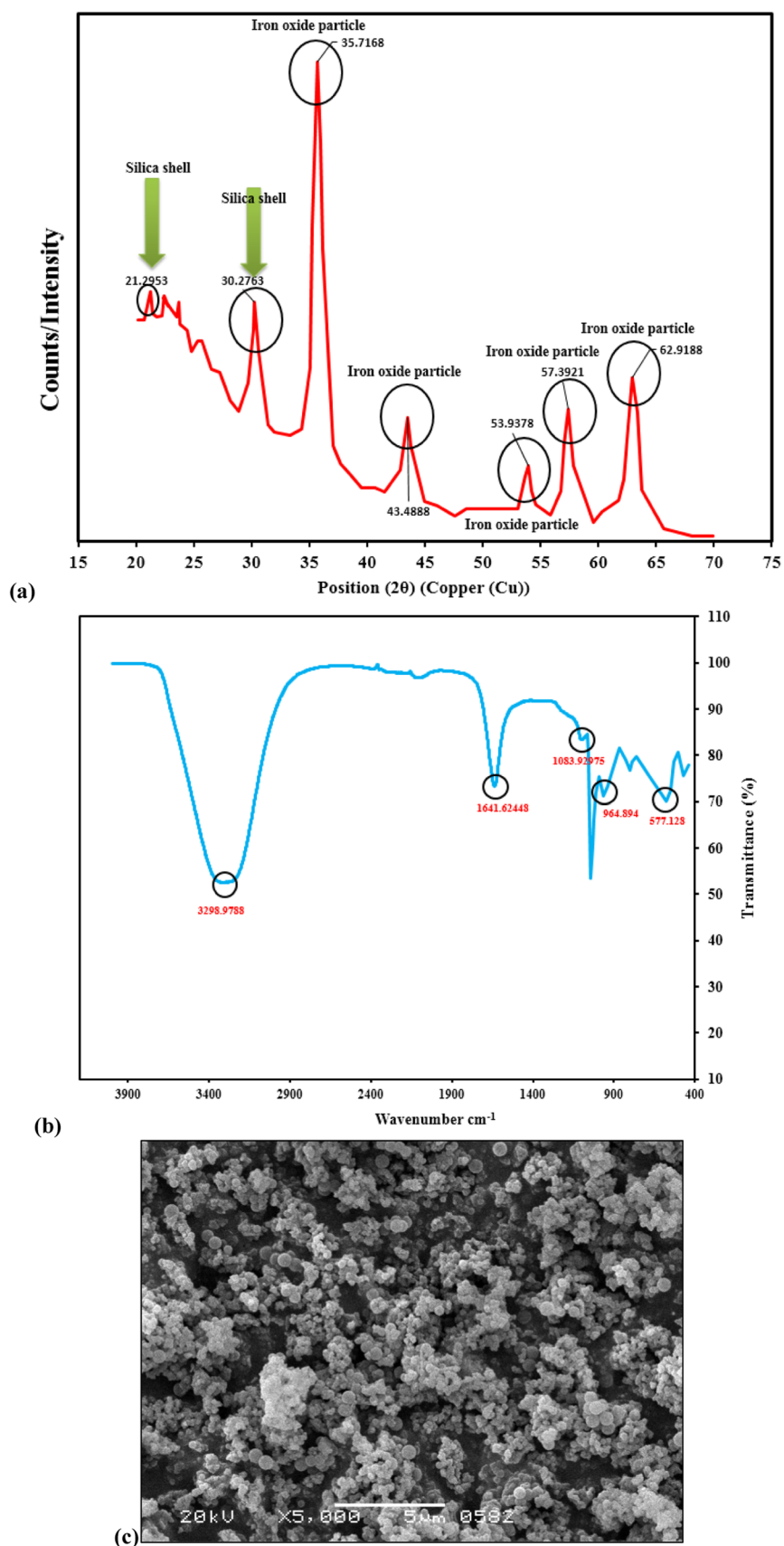
**Table 2** Composition of all the samples prepared in this study

Components	BM$_1$	BM$_2$	BM$_3$	KCl$_1$	KCl$_2$	MgCl$_1$	MgCl$_2$	NaCl$_1$	NaCl$_2$
Tap water (mL)	310	310	310	310	310	310	310	310	310
KCl (g)	18	18	18	18	18	18	18	18	18
MgCl$_2$ (g)	18	18	18	18	18	18	18	18	18
NaCl (g)	18	18	18	18	18	18	18	18	18
PAC (g)	3	3	3	3	3	3	3	3	3
Soda ash (g)	0.25	0.25	0.25	0.25	0.25	0.25	0.25	0.25	0.25
Xanthan gum (g)	0.5	0.5	0.5	0.5	0.5	0.5	0.5	0.5	0.5
Barite (g)	82	82	82	82	82	82	82	82	82
Nanoparticles (g)	X	X	X	0.875	1.75	0.875	1.75	0.875	1.75

BM base mud
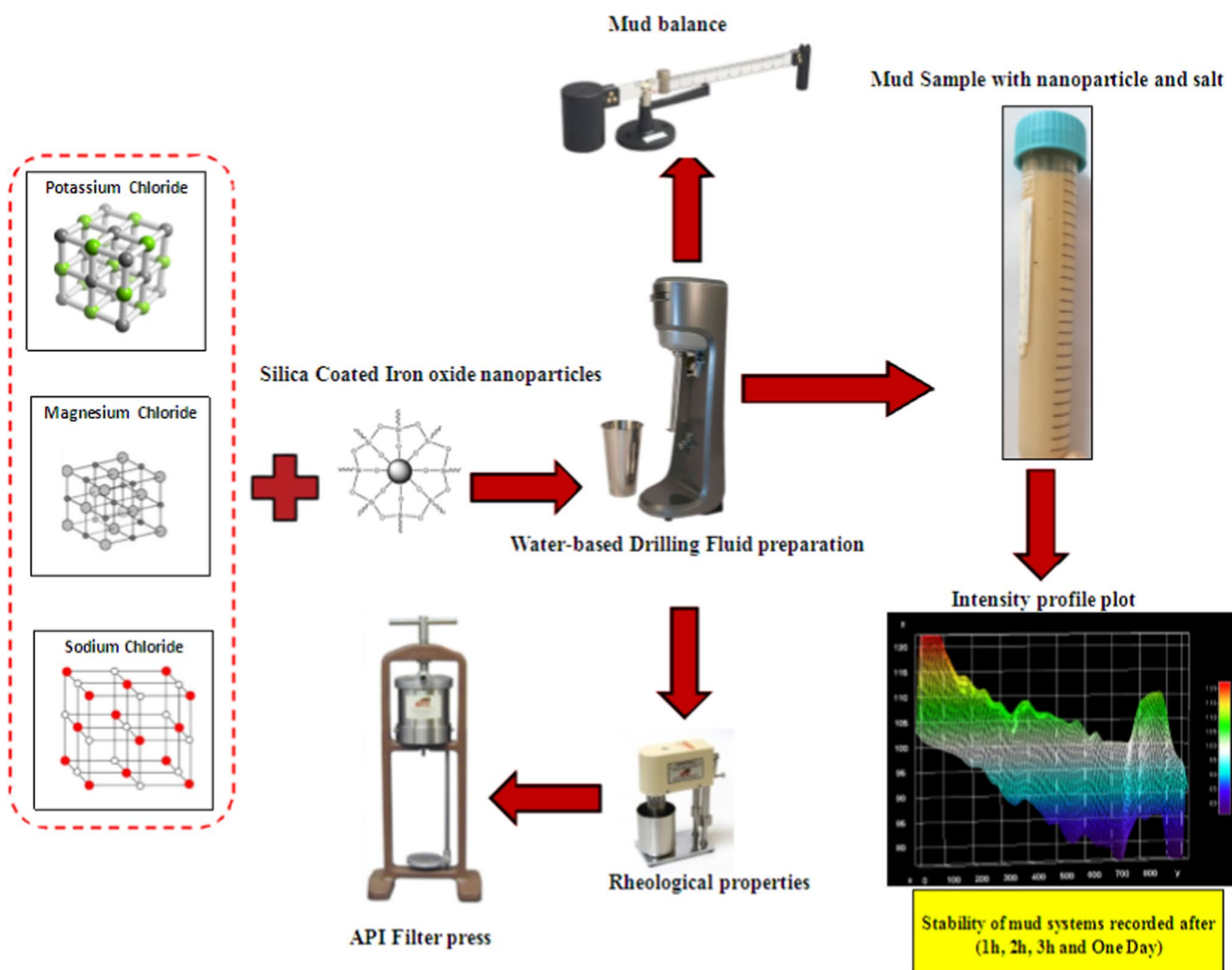
Fig. 3 Testing procedure followed during the study

(a)

(b)

(c)

(d)
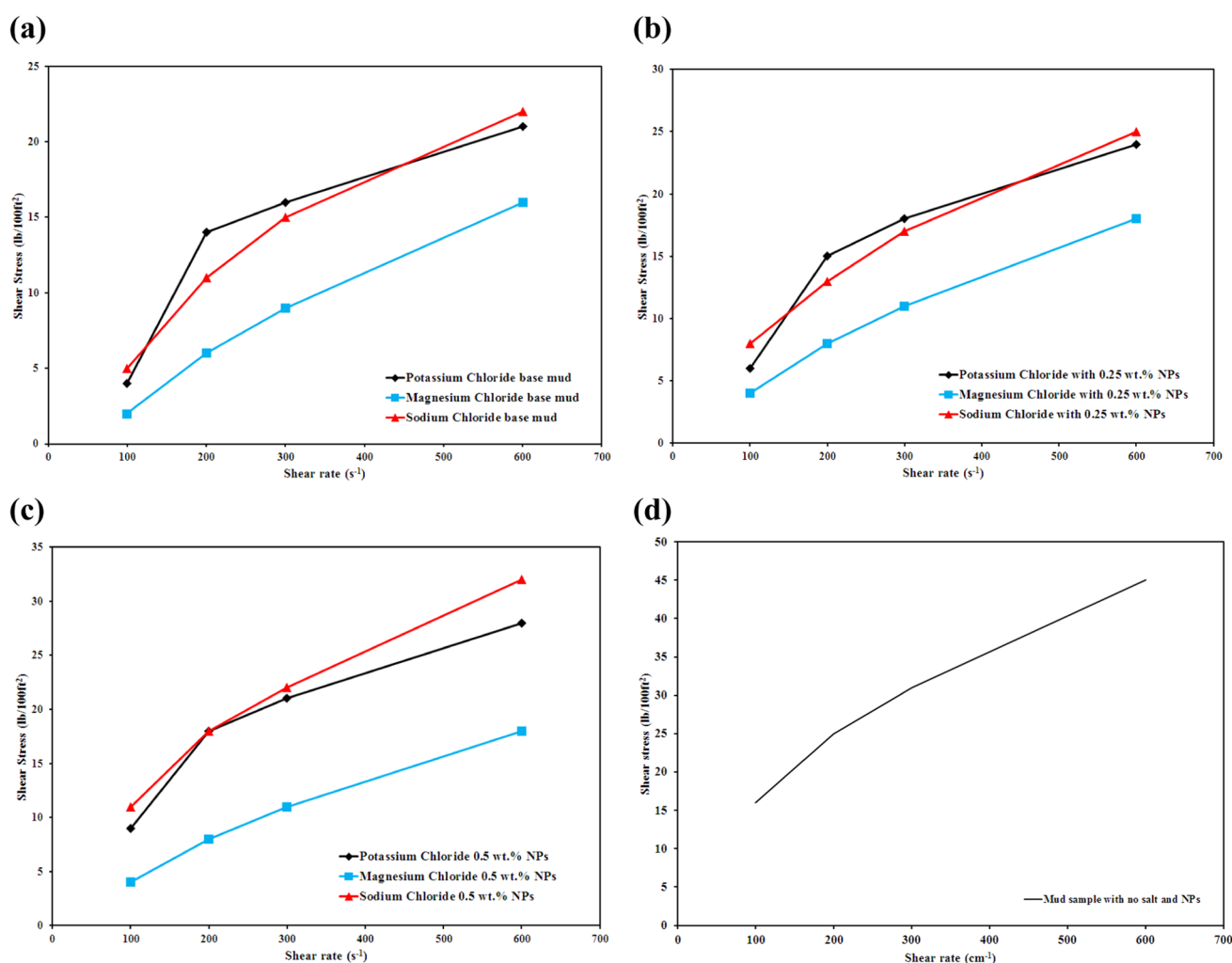
Fig. 4 Rheogram of drilling fluid. **a** Base mud with no NPs, **b** 0.25 wt.% of NPs and salts, **c** 0.5 wt.% of NPs and salts, **d** no salt and NPs

the researcher to observe the changes in mud and mud cake during the stopping of the drilling operation, as a result of any unforeseen drilling event.

Materials and methodology

Materials

The materials used for the synthesis of nanoparticles and water-based mud systems are shown in Table 1. Some of the materials were acquired from local vendors while others were obtained directly from a service company.

### Synthesis of Si/Fe$_3$O$_4$ nanoparticles

The Si/Fe$_3$O$_4$ nanoparticles in this article were synthesized using the modified Stober method. Figure 1 shows the procedure used for the preparation of Si/Fe$_3$O$_4$ nanoparticles.

Initially, a solution of Fe$_3$O$_4$ nanoparticles and ethanol-RO water was prepared with a volume ratio of 10:1 (Ng et al. 2020). The prepared solution was sonicated for 30 min in ultrasonic bath, and after sonication, different concentrations of tetraethyl orthosilicate (TEOS) were added in the solution. By using ammonia, the pH of the mixture was sustained at 11. The reaction was continued at ambient condition for 12 h with constant stirring. Once the reaction is completed, the Si/Fe$_3$O$_4$ nanoparticles were separated from the mixture using a neodymium magnet. The recovered particles were then washed with ethanol-RO water for tuning the nature of supernatant. The washed particles then dried for one day at -45 °C and then used for further investigation.

Characterization of nanoparticle

Figure 2 shows the characterization of silica-coated iron oxide nanoparticles. Figure 2a presents the XRD analysis. This test is mainly used to investigate the composition

Fig. 5 Mud weight of the samples after variation in salt type and NPs concentration
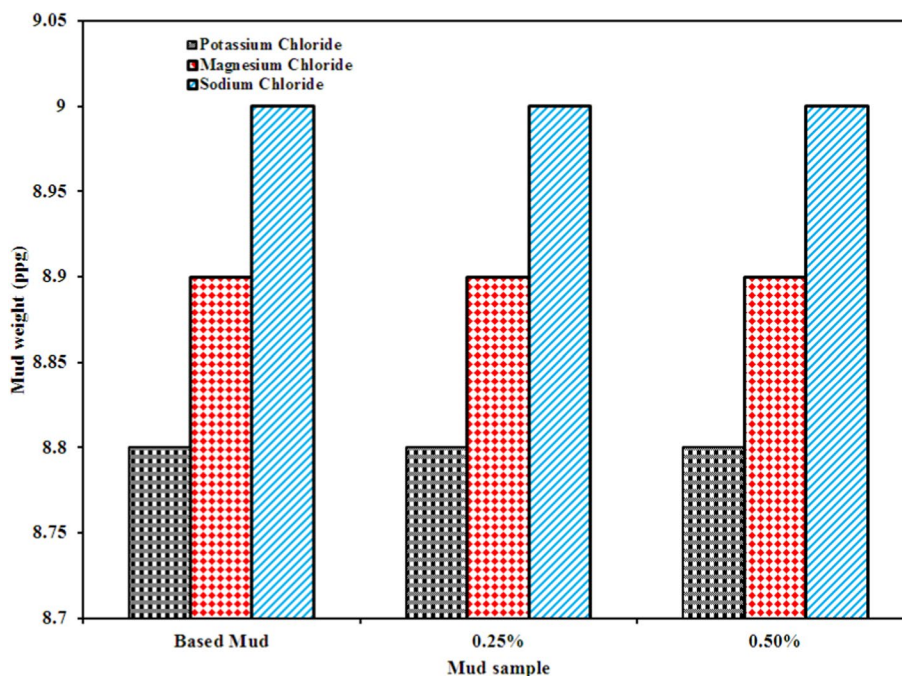
associated with any material (Aftab et al. 2016). The diffraction peaks at 35.716°, 43.488°, 53.937°, 57.391°and 62.918° represent the planes of cubic inverse spinel of iron oxide (Asab et al. 2020). Moreover, the peaks at 21.295° and 30.276° indicate the presence of silica shell coating on the magnetic nanoparticles. The coating of silica over the iron oxide nanoparticle also increases the crystallite size of the iron oxide particle. In addition, the zeta potential of the particle was also tested using an aqueous solution. The nanoparticle gave a value of -33.37 ± 0.38 mV.

Figure 2b shows the FTIR spectrum of the synthesized particle. With the help of the infrared absorption spectrum, chemical bonding within a molecule can be determined. The peak detected at 577.128 cm^{-1} shows the Fe–O bond present within the nanoparticles. The high absorption peak at 3298.978 cm^{-1} and 1641.624 cm^{-1} shows the bending and stretching vibration of—OH bond within the molecule (Ullah et al. 2014). The band at 964.89 cm^{-1}was assigned to the stretching vibration of the Si–OH bond. On the other hand, the peak at 1083.93 cm^{-1} represents the asymmetric linear vibrations associated with Si–O–Si (Asab et al. 2020). All these absorption peaks indicate the successful formation of silica shells over iron oxide nanoparticles (Villa et al. 2016).

Figure 2c depicts the scanning electron microscope imaging of the nanoparticles. This test shows the morphology of the synthesized particle (Aftab et al. 2016). The spherical shape in the form of glass beads quite evident from the closer assessment of the particle.

Preparation of drilling fluid samples

Preparation and testing of the drilling fluids were conducted as per API 13B1 recommended practices for testing water-based drilling fluids. During experimentation, 1 barrel equivalent to 350 cc was prepared using 310 mL of tap water, 0.25 g of soda ash (Na$_2$CO$_3$), 18 g of salt, 3 g of PAC, 0.5 g of xanthan gum and 82 g of barite. Three salts, KCl, NaCl and MgCl$_2$, were also used in this formulation. 18 g of each salt was added in the mud system as a shale inhibitor. In addition, silica-coated iron oxide nanoparticles were added in two different concentrations of 0.25 and 0.5 wt.%, respectively, in the solution. The performance of this nanoparticle was investigated under the influence of different salts. The silica-coated iron oxide nanoparticles were synthesized using the modified Stober method. Six different mud samples were formulated in the laboratory, and it was ensured that all these nine samples received identical testing methods and treatment. Table 2 and Fig. 3 show the number of samples with their composition and the experimentation flow work followed during the course of the study, respectively.

Mud density measurement

Once the samples were formulated, the mud weight of each sample was obtained using the OFTIE mud balance. The mud weight of each sample was reported in pounds per gallon (ppg). Mud bearing low density can cause problems related to washout or caving that ultimately lead to loss of

(a)

(b)

(c)

(d)

(e)

(f)

(g)
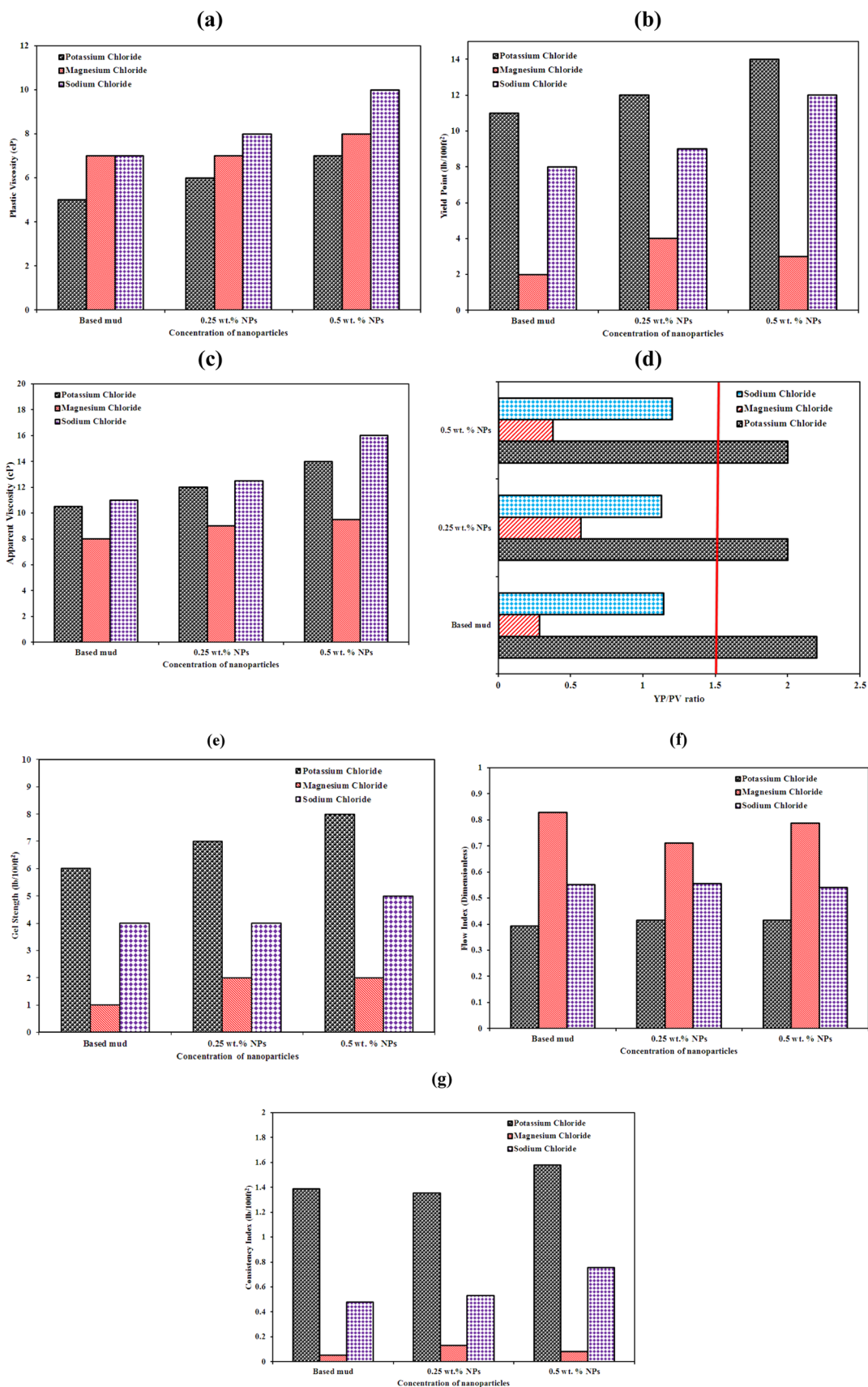
◄**Fig. 6** Rheological properties after changing salt type and concentration of the NPs. **a** Plastic viscosity, **b** yield point, **c** apparent viscosity, **d** YP/PV ratio, **e** gel strength, **f** flow index, **g** consistency index

wellbore integrity in the form of wellbore collapse. On the other hand, high mud weight usually increases the loss of circulation and formation damage, and decreases the rate of penetration (ROP).

Rheological parameters

A six speed FANN 35 rheometer (600, 300, 200, 100, 6 and 3) RPMs were used to measure the rheological characteristic of each of the studied samples. Rheological properties that include plastic viscosity, yield point, apparent viscosity and gel strength were obtained at ambient conditions. The cup of viscometer was filled to the prescribed line with each sample, and the rotor of the viscometer was submerged into the drilling fluid. The rotor was rotated at four different RPMs till the reading on the meter stabilized. Once these readings were obtained, the flow characteristics were determined using the correlations as shown in Eqs. (1)–(3) (Bég et al. 2018):

$$\text{Plastic Viscosity (cP)} = 600 \text{ RPM reading} - 300 \text{ RPM reading} \quad (1)$$

$$\text{Yield Point } \frac{\text{lb}}{100 \text{ ft}^2} = 300 \text{ RPM reading} - \text{PV} \quad (2)$$

$$\text{Apparent Viscosity (cP)} = \frac{600 \text{ RPM reading}}{2} \quad (3)$$

$$\begin{aligned} &\text{Gel Strength } \frac{\text{lb}}{100 \text{ ft}^2} \text{ recorded directly from the viscometer} \\ &\quad \text{at 3 RPMafter the mud was in static condition} \\ &\quad \text{for a period of 10 s} \end{aligned} \quad (4)$$

API LPLT filter press

The filtration tests were performed according to API recommended standards. Each test was conducted at room temperature and pressure conditions (25 °C and at 1 atmosphere). A given sample of mud was placed in the API filter press cell, and a differential pressure of 100 psi was supplied for 30 min. Loss of filtrate volume that was collected in the graduated cylinder was recorded, and the mud cake at the end of the experimentation was collected. The filter cake was placed under the atmospheric environment to evaporate any water molecules present. Small weights are placed at the end of the filter paper to prevent it from curling during the evaporation process. Inert gas in the form of nitrogen is

applied, so that no chemical reaction takes place between the molecules of the mud and the gas. The uncertainty during the testing process was kept under 2%.

Result and discussion

Shear stress verses shear rate (rheogram)

The rheogram of all the mud samples was obtained using a FANN 35 rheometer. Figure 4a–d depicts the graphical representation between shear stress and shear rate of all the samples obtained using the power law model. All the samples show shear thinning characteristics, which will result in the higher viscosity of the sample at lower shear rates (Li et al. 2015). Drilling mud that demonstrates adequate shear thinning characteristics is better to circulate within wellbore and it is extensively used in increasing the drilling efficiency (Rafieefar et al. 2021). Moreover, it was observed that effect of salts reduces the rheogram and lower it down as compared with the rheogram of the salt-free system. This was in good agreement with the study conducted by Rezaei et al. (2020). This reduction in the shear stress of the system is due to the neutralization of the negative charges associated with the base mud system (Rezaei et al. 2020). Disruption of xanthan gum charges takes place as a result of K^+, Na^+ and Mg^{2+} ions present in the mud. The negative charge of xanthan gum-water suspension has already been proved through the zeta potential test (Brunchi et al. 2016). The presence of cationic salts results in the disruption of xanthan gum charge balance, and the contraction of its chain, which is in the form of a rigid worm-like structure in solution. The interaction ultimately reduces its shear stress and viscosity (Bewersdorff and singh 1988).

Figure 4a–c depicts that the minimum reduction in the rheogram was in monovalent cations followed by divalent cations (Rezaei et al. 2020). These monovalent ions demonstrate weaker behavior in neutralizing the xanthan gum suspension. In addition, the proportional increase in shear stress is observed as the concentration of the nanoparticles increases in salt systems. The addition of nanoparticles changes the net charge to positive in the xanthan gum-water system. These cation-NP systems get more stable with the addition of NPs.

Density of mud samples

Mud weight is an important feature of drilling fluid, which not only acts as a primary barrier in the wellbore but also maintains the hole integrity. This parameter is measured using the mud balance equipment. This instrument is extremely reliable and fast in determining the density of the
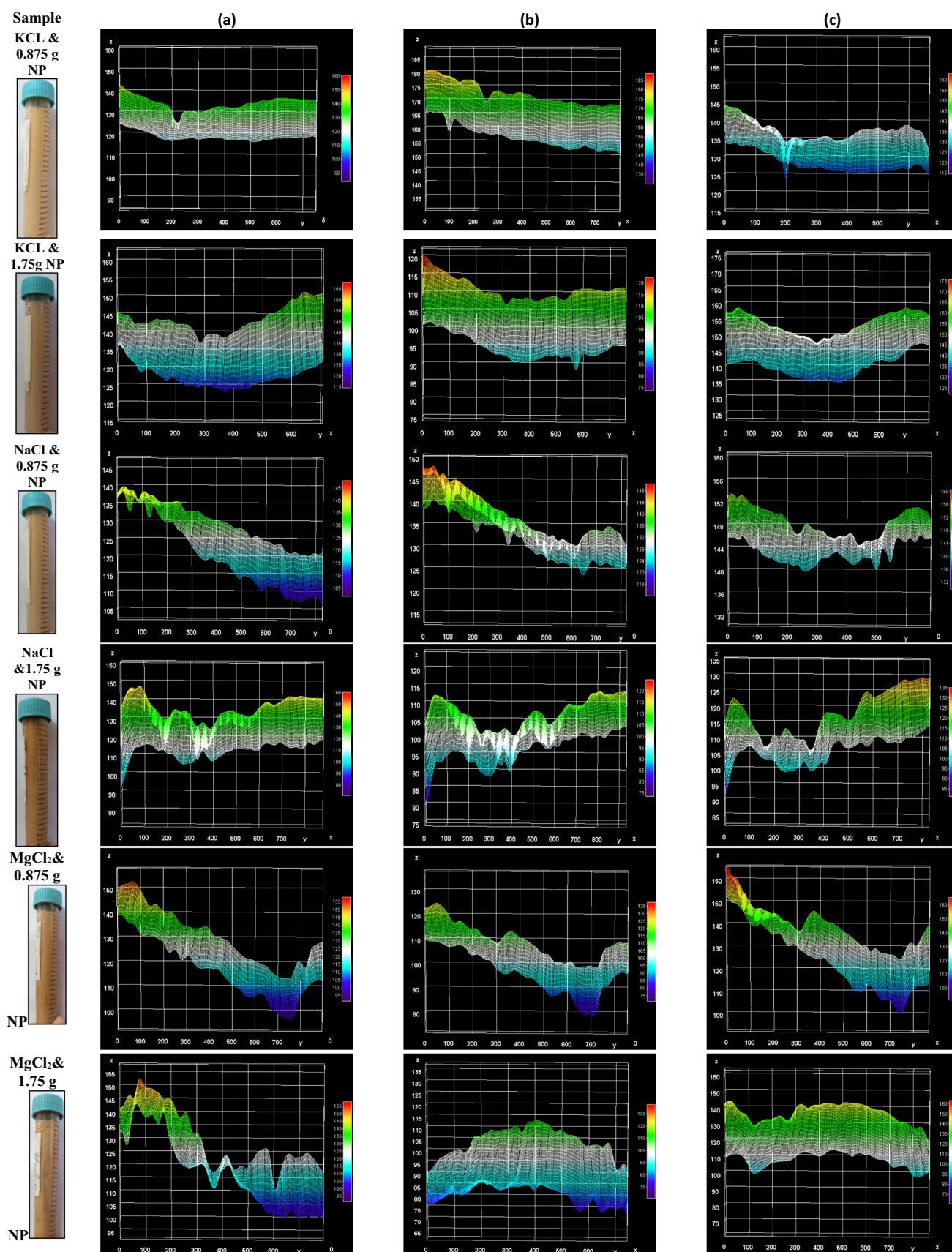
Fig. 7 **a–c** Stability of mud systems after interaction between different cations and nanoparticles. **a** 1 h, **b** 2 h, **c** 3 h

mud system. No external effects like temperature and pressure can influence the mud weight of a system (Lalji et al. 2022a). Figure 5 shows the mud density in ppg of all the 09 samples. No substantial changes in the density of the mud system were evident with a rise in concentration of the silica-coated iron oxide nanoparticles. This similar experience was noted by Rafieefar et al. (2021); his research focuses on different nanoparticles. The density of all the samples was in the range of 8.8–9 ppg, which is also counted as an appropriate range of mud weight after the addition of nanoparticles (Ikram et al. 2021). Moreover, no substantial changes in mud weight was evident with the changes in cations in the mud system. The trends in this study are similar to the study conducted by Alireza et al. (Lalji et al. 2022a).

Rheological properties of the systems

Figure 6a–d depicts the rheological properties of the mud system with the changes in cations and the addition of nanoparticles. Figure 6a presents the plastic viscosity (PV) of all the samples in the study. This parameter is produced between the fluid layers and the solid particles present in the mud system (Rafieefar et al. 2021). It was noted that with the rise in NPs concentration of within the fluid, PV of the system increases. The improvement is, because of the rise in solid content within the mud, which affects the friction present in the mud system (Lalji et al. 2022a). Moreover, NPs separate the xanthan gum flocculation, which ultimately enhances the PV of the system. The spherical shape of nanoparticles depicted in Fig. 2c was easy to disperse throughout the fluid system, which eventually increased the PV. The smaller size particles exhibit stronger interaction between one another compared with the larger size particles, and eventually it increases the viscosity (Wang et al. 2012). Moreover, the higher negative zeta potential demonstrated by the nanoparticles creates a strong repulsive forces against the negatively charged xanthan gum, which inhibits the free flowing motion of the particles and eventually increases PV. The highest PV of 10 cP was observed in monovalent cation of sodium, while for divalent cation the maximum PV was 8 cP.

Figure 6b shows the yield point (YP) of all the systems. This feature of drilling fluid ensures the suspension of drilling cutting in the wellbore during static and circulating conditions (Rafieefar et al. 2021). It is formed by the attractive forces between the negative and positive charges (Lalji et al. 2023). At a higher yield point efficiency of the cutting transportation will increase. Nevertheless, if it goes beyond the range then excessive pumping pressure is necessary to initiate the circulation (Ismail et al. 2016). The YP of the salt-free and no NP system was 17 lb/100 ft^2. This factor reduces with the addition of cations in the mud system. This reduction is mainly because of the elimination of forces of attraction by the addition of cations (Lalji et al. 2022a).

On the other hand, an increase in the concentration of the NPs enhances the YP of the system (Lalji et al. 2022a). The lower than -30 mV zeta potential of the particle indicates a higher stability of the nanoparticles in the suspension (Ho et al. 2019). The -33.37 ± 0.38 mV magnitude shows higher stability and dispersion of nanoparticles in the mud system. These NPs can improve the attractive forces in the fluid system and that subsequently increases the YP (Lalji et al. 2022a).

Figure 6c presents the apparent viscosity (AV) of all the systems. This parameter is only evaluated for non-Newtonian fluid systems. As the concentration of silica-coated iron oxide nanoparticles increases, AV of the systems starts to improve (Lalji et al. 2022a). This important finding shows that these nanoparticles possess capability to support xanthan gum in any drilling environment. Moreover, it was observed that the sodium ion has the minimum influence on the AV of the system. This ion has less positive charge as compared with magnesium ions. In addition, as the size of monovalent cation increases a greater reduction in AV is observed. The ionic radius of potassium ions is greater than sodium; hence, the reduction is higher in K$^+$ ions. Therefore, it can be concluded that NPs have more influence on AV in comparison with the changes in salt.

Figure 6d shows the ratio of YP and PV of all the samples. According to APT 13A specification, the recommended magnitude for this ratio is 1.5 (Elkatatny 2019). A drilling fluid that enables this ratio value will demonstrate higher cutting carrying capacity and effective hole-cleaning characteristics. It was observed that monovalent cations, especially K$^+$ obtained YP/PV ratio greater than the recommended magnitude. This clearly shows that this system of mud will reduce drilling problems that arise due to cutting accumulation and differential sticking (Elkatatny 2019).

Gel strength (GS) signifies the capacity of drilling fluid to suspend the drill cutting under static conditions (Bayat et al. 2018). This ability arises because of the electrochemical forces of attraction present within the fluid system when it experiences a static condition (Bayat et al. 2018). Figure 6e depicts the gel strength of all the systems measured at 10 s. It was observed that as the concentration of NPs increases, GS also elevates. The result is similar to the Ali Reza et al. study (Rezaei et al. 2020), where only iron oxide NPs are used to investigate the effect on GS. The silica-coated iron oxide NPs also demonstrate similar characteristics. In addition, the monovalent cations show higher GS values than divalent cations. The highest GS value was obtained from K$^+$ ion followed by Na$^+$ and then Mg^{2+}. This clearly indicates that as the ionic radius increases, GS also intensifies.

Figure 6f, g shows the power law parameters obtained for all the samples in this study. These parameters show the nature and characteristics of drilling fluid under observation. The dimensionless flow index parameter shown in Fig. 6f

Stability of mud after One Day
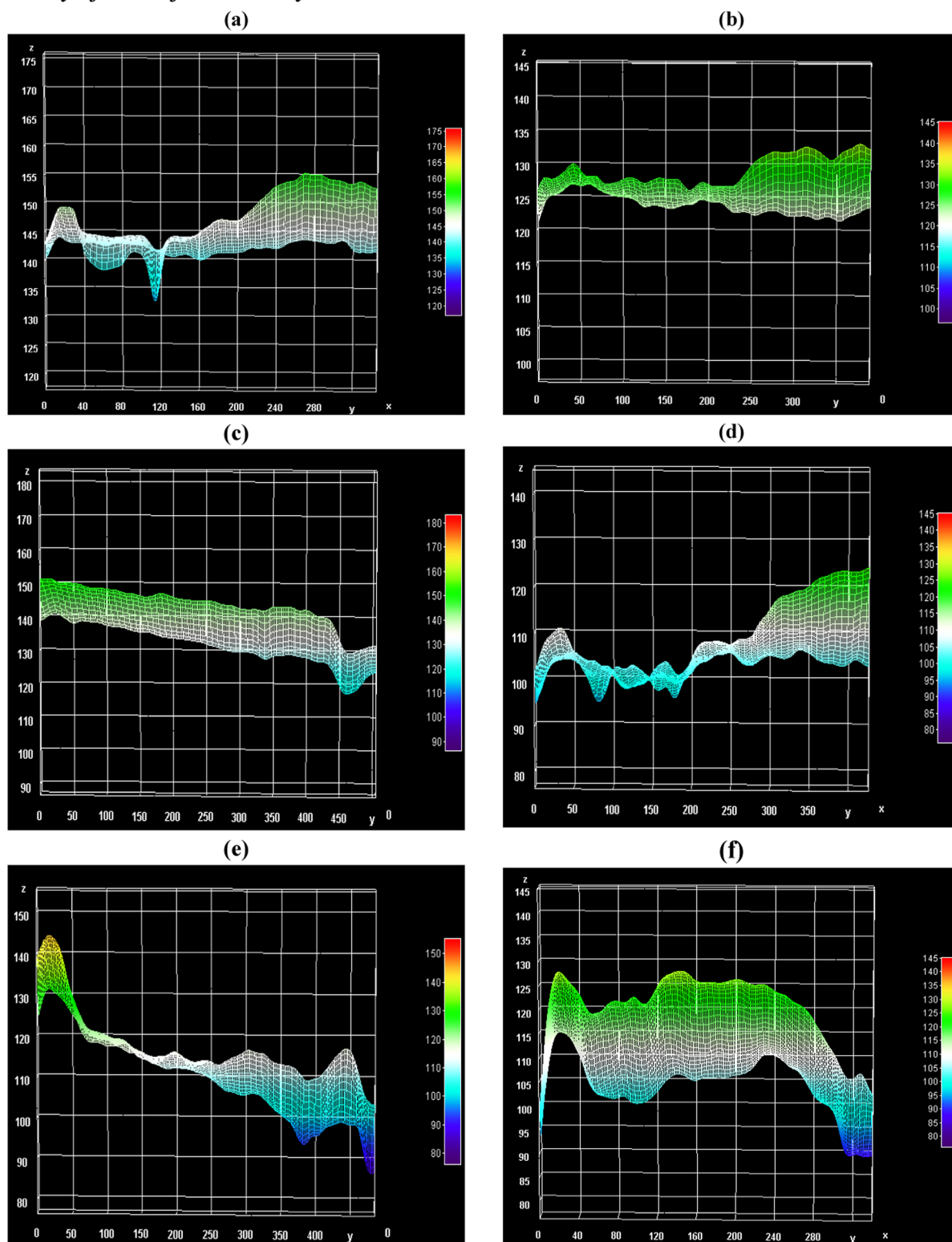
Fig. 8 Intensity profile plots showing the stability of mud systems. **a** KCL and 0.875 g NP, **b** KCL and 1.75 g NP, **c** NaCl and 0.875 g NP, **d** NaCl and 1.75gNP, **e** $MgCl_2$ and 0.875 g NP, **f** $MgCl_2$ and 1.75 g NP

Fig. 9 Influence of cations and nanoparticles on the API LPLT filtrate loss
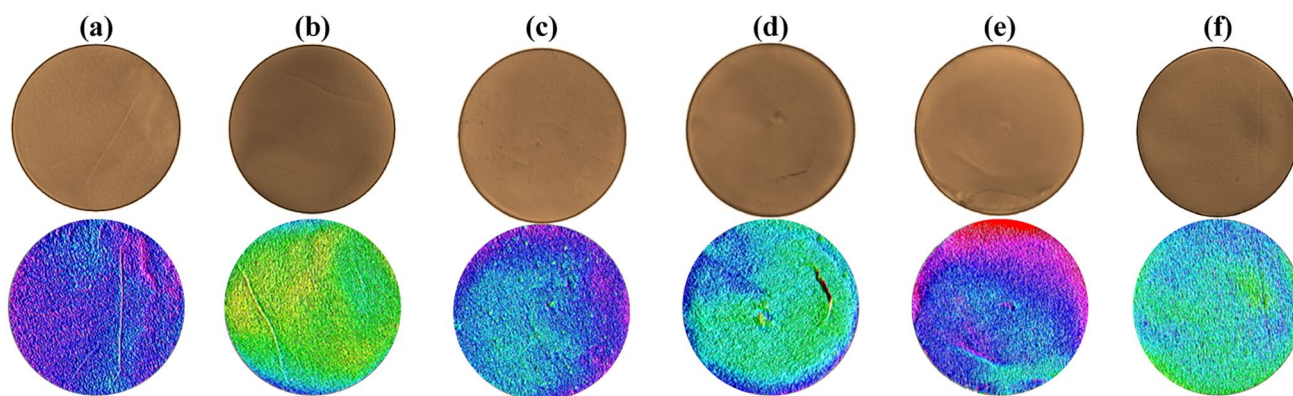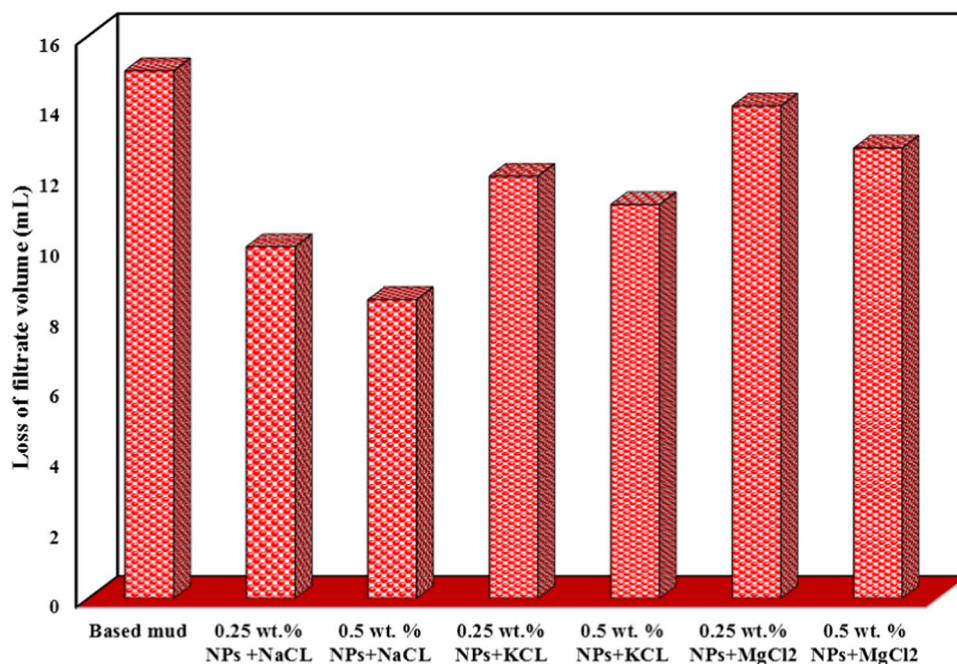
Fig. 10 Visual representation of mud cake and its surface plots. **a** KCl and 0.875 g NPs, **b** KCl and 1.75 g NPs, **c** NaCl and 0.875 g NPs, **d** NaCl and 1.75 g NPs, **e** MgCl$_2$ and 0.875 g NPs, **f** MgCl$_2$ and 1.75 g NPs
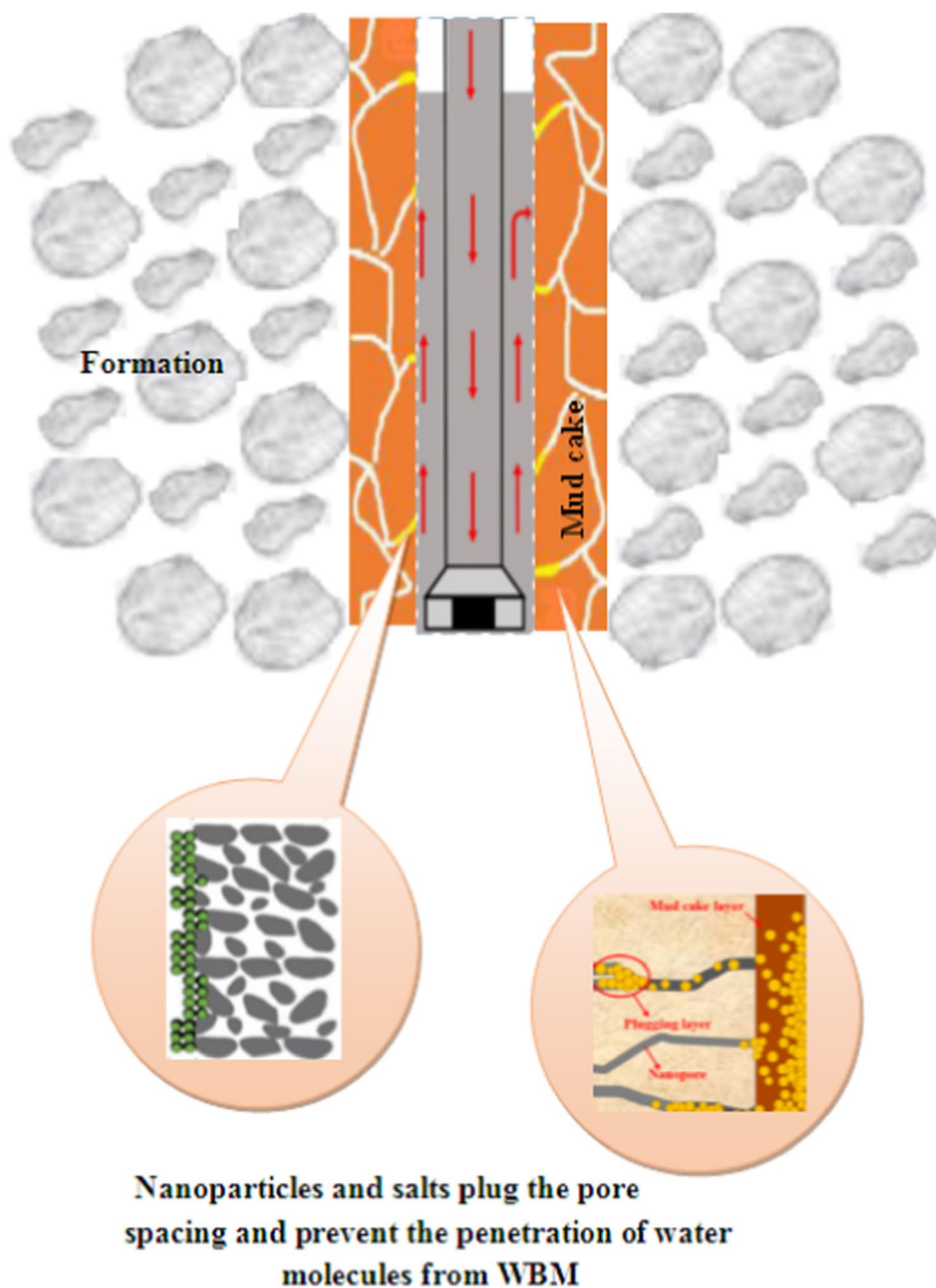
indicates that all the samples in this study are shear thinning/pseudo plastic fluid with a value lower than 1 in each case. This also validates the rheogram results obtained in Fig. 4. On the other hand, the consistency index factor as shown in Fig. 6g usually specifies the thickness of the mud cake. The higher the value, the more capable the mud will be in carrying the cutting up to the surface. It was noted that the K$^+$ mud was the most favorable of all the samples. It was followed by sodium and then magnesium ions. Furthermore, as the concentration of the NPs increases, an increase in consistency factor was also recorded in each sample cation. Hence, these results clearly show that silica-coated iron oxide NPs can be considered as a good additive in increasing the cutting carrying capacity of drilling fluids.

Stability analysis of different mud samples using image processing technique

Figure 7a–c presents the stability of the mud systems monitored after three consecutive hours. Silica-coated iron oxide nanoparticles were added in two different concentrations 0.875 g and 1.75 g in the based mud system. Two samples of each salt were prepared and monitored for their stability under static conditions. No change in the intensity profile trend was recorded for potassium chloride salt. At both

Fig. 11 Effect of salt and nanoparticles on the wellbore stability

Nanoparticles and salts plug the pore spacing and prevent the penetration of water molecules from WBM

concentrations of nanomaterial, this salt provides a similar intensity profile for three consecutive hours. The change noticed was in the amplitude of the intensity, which might be because of the light source present in the surroundings. A similar characteristic was observed in sodium chloride salt with lower nanoparticle concentration. This sample illustrates a decreasing trend in its intensity profile, which will be due to the solid particle at the lower half of the test tube. Moreover, some bubbles in the mud were also noticed which is apparent by the fluctuations recorded at the beginning. However, as the concentration of nanoparticles is increased in the sodium chloride salt system, the stability of the mud

was achieved throughout experimentation, which can be observed with the horizontal trend in the intensity profile plots. Analogous behavior was also witnessed in magnesium chloride salt at both nanoparticles concentrations.

Stability of mud after one day

Figure 8a–f shows the intensity profile plots after one day of experimentation. The testing was performed under static ambient conditions. Figure 8a, b presents the stability of mud composed of KCl and different concentrations of nanomaterial. No substantial changes were noticed in these

samples. They demonstrate similar intensity profiles as it was recorded during the first three hours of mud preparation. Figure 8c, d depicts the intensity profiles of sodium chloride salt. The sample in Fig. 8c shows that at lower concentration of nanoparticles, an inclination is observed in its profile. Moreover, dephasing was also noticed, which is witnessed with a decrease in profile plot toward the later end of the profile. However, as the concentration of nanoparticles is increased stability is achieved, which can be observed with a horizontal contour. For $MgCl_2$ as shown in a Fig. 8e, dephasing of the mud was detected at the start of the profile. A marked increase in intensity was recorded; this indicates the transmission of light to the transparent phase. The profile starts to decline throughout the test tube, which is due to the settling of solid particles in this sample. Figure 8f shows $MgCl_2$ with higher concentrations of NPs. This sample shows three distinct behaviors in its test tubes. Dephasing was noticed at the start of the test tube which was recorded as a higher intensity profile, then the stable region with no substantial change and the settling of particles, which was associated with a decrease in profile. Hence, it can be concluded that KCl salt should be used in the silica-coated iron oxide nanoparticle mud system.

Fluid filtration characteristics

Penetration of fluid into any formation results in the loss of wellbore integrity and causes severe wellbore instability issues (Fattah and Blkoor 2013). In addition, this migration causes an increase in the thickness of the mud cake, which is the main source of pipe sticking problems (Fattah and Blkoor 2013). The efficacy of any fluid can be judged based on the loss of filtrate volume and the shape and texture of the mud cake. The quantity of the loss from each sample during this study is shown in Fig. 9. The base mud sample with no salt and no nanoparticles demonstrated the highest filtrate loss volume of 15 mL after standard 30 min of testing. When different cationic salts and Si/Fe_3O_4 nanoparticles were introduced in the system, a drastic reduction in filtrate loss was observed. Moreover, as the concentration of these two entities increases in the mud system, more reduction in filtrate volume loss was recorded. The minimum loss was displayed by NaCl + Si/Fe_3O_4 combination (Kuma et al. 2020). The micropores are plugged by sodium salt, whereas the nanopores are blocked by Si/Fe_3O_4. Mg^{2+} salt shows the least efficiency in terms of minimizing the filtrate loss as it demonstrated a maximum fluid loss volume of 14 mL/30 min in comparison with other salts. However, as the concentration of Si/Fe_3O_4 increases, this volume reduces to 12.8 mL/30 min. When the fluid was saturated with potassium salt, it showed 12 mL/30 min and 11.2 mL/30 min of fluid loss for 0.25 and 0.5 wt.% of Si/Fe_3O_4, respectively. At higher

concentrations, the nanoparticles physically plug the pore spacing and prevent the penetration of filtrate. This filtration test result is in good agreement with the study conducted by Kuma et al. (2020). Moreover, the reduction in filtrate volume is mainly experienced due to the electrostatic repulsion between the negatively charged xanthan gum and nanoparticles. These repulsive forces prevent the flocculation of particles in the mud system and at the same time maintain particles in a well-dispersed phase in the mud.

Figure 10 depicts the shape and texture of the mud cake obtained from the API filter press test. These mud cakes were dried in an open environment for 24 h before being investigated further. As the concentration of Si/Fe_3O_4 increases, the color of the filter cake becomes intense. All the filter cakes were compacted. The presence of xanthan gum assists Si/Fe_3O_4 nanoparticles in forming a firm barrier onto the filter paper. The spherical beads shaped Si/Fe_3O_4 nanoparticles create a stiff bonding with the polymeric chain of xanthan gum and make the mud cake smooth and compacted.

Figure 10 also shows the surface plots of each mud cake used to analyze the mud cake surface texture. The mud cake surface plots were obtained from ImageJ, an image processing tool. The ImageJ software was mainly used to have a more comprehensive knowledge of the mud cake surface, which is impossible to detect from the naked eye. The presence of fractures, cracks and any other surface damage were all recorded during this investigation.

The dark and lighter colors indicate high and low intensity regions, respectively. These intensities mainly depended on the transmission of light. It is evident from Fig. 10 that as the concentration of Si/Fe_3O_4 increases the mud cake becomes more compacted and it displays more compacted regions. A similar trend was observed in each of the cations. Furthermore, any fractures, fissures and damage to the mud cake can also be identified using these plots. Some fractures are detected in Fig. 10a, b, d, e. In surface plots, these fractures were discovered to have high intensities.

Figure 11 presents the mechanism behind the minimum fluid loss in the presence of salt and nanoparticles. The combined effect of salt and nanoparticles substantially reduces the fluid loss volume and produces thin and compacted mud cake (Vryzas and Kelessidis 2017). Deterioration in the performance of salt is observed when it is used as a separate entity. The nanoparticles not only fill the micron spacing, but they can also plug the nanopores (Vryzas and Kelessidis 2017). During the fluid loss process, numerous nanoparticles work collectively. They move inside the pore spacing where the larger diameter salt particles cannot move, and seal the spacing by the phenomena of pore bridging. The high surface area-to-volume ratio and spherical nature of these particles enable them to be an effective plugging agent.

Conclusion

The study was conducted to investigate the performance of Si/Fe$_3$O$_4$ in the presence of different cationic salts. Rheological and filtration tests were conducted to understand the efficacy of Si/Fe$_3$O$_4$ nanoparticles in improving the characteristics of water-based mud. The coating of iron oxide nanoparticles with silica was a successful approach in reducing the coagulation of iron oxide nanoparticles, which increases the efficiency of the water-based mud. During the experimentation, the presence of different cationic salts was also investigated. The addition of salt reduces the rheogram and moves it down as compared with the rheogram of the salt-free system. The reduction of shear stress in the salt system is mainly because of the neutralization of the negative charges associated with the base mud system. However, this behavior was weaker in monovalent cations as compared with the divalent. Substantial improvement in mud rheological properties due to high stability and dispersion of nanoparticles in the mud system was also recorded. Moreover, the stability analysis shows that the mixture of KCl and NPs proves to be the best in terms of achieving a stable mud system. No significant changes in the mud stability were recorded. The mud demonstrated good stability even after one day. Furthermore, the combination of salt and spherical shape nanoparticles was extremely effective in reducing the filtrate loss volume. Both these entities physically plug the pore spaces and prevent fluid loss from the mud. Based on the findings, it can be concluded that the mixture of salt and Si/Fe$_3$O$_4$ nanoparticles improves the behavior of WBDFs.

Declarations

Conflict of interest The authors declare that they have no conflict of interest.

References

Afolabi RO, Orodu OD, Seteyeobot I (2018) Predictive modelling of the impact of silica nanoparticles on fluid loss of water based drilling mud. Appl Clay Sci 151:37–45

Aftab A, Ismail AR, Khokhar S, Ibupoto ZH (2016) Novel zinc oxide nanoparticles deposited acrylamide composite used for enhancing the performance of water-based drilling fluids at elevated temperature conditions. J Petrol Sci Eng 146:1142–1157. https://doi.org/10.1016/j.petrol.2016.08.014

Ahmad HM, Kamal MS, Al-Harthi MA (2018) High molecular weight copolymers as rheology modifier and fluid loss additive for water-based drilling fluids. J Mol Liq 252:133–143

Ali JA, Ahmed RN, Abdullah AD, Ali NH, Kalhury AM, Sabir AN, Manshad AK, Keshavarz A, Amir H (2022) Development of a nanobiodegradable drilling fluid using prosopis farcta plant and pomegranate peel powders with metal oxide nanoparticles. ACS Omega Mohammadi 7(35):31327–31337

Al-Saba, MT, Al Fadhli A, Marafi A, Hussain A, Bander F, Al Dushaishi MF (2018) Application of nanoparticles in improving rheological properties of water based drilling fluids. SPE Kingdom of Saudi Arabia Annual technical symposium and exhibition

Alyasiri M, Antony J, Dongsheng W (2017) Enhancement of drilling fluid rheology by nanoparticles. Annu Trans Nord Rheol Soc Wen 25:349–351

Asab G, Zereffa EA, Seghne TA (2020) Synthesis of silica-coated Fe$_3$O$_4$ nanoparticles by microemulsion method: characterization and evaluation of antimicrobial activity. Int J Biomater 2020:4783612. https://doi.org/10.1155/2020/4783612

Awele N (2014) Aalborg University Esbjerg. Investigation of additives on drilling mud performance with" tønder geothermal drilling" as a case study

Bayat AE, Moghanloo PJ, Rafati APR (2018) Experimental investigation of rheological and filtration properties of water-based drilling fluids in presence of various nanoparticles. Colloids Surf A 555:256–263. https://doi.org/10.1016/j.colsurfa.2018.07.001

Bég OA, Espinoza DES, Kadir A et al (2018) Experimental study of improved rheology and lubricity of drilling fluids enhanced with nano-particles. Appl Nanosci 8:1069–1090. https://doi.org/10.1007/s13204-018-0746-4

Bewersdorff H-W, Singh RP (1988) Rheological and drag reduction characteristics of xanthan gum solutions. Rheol Acta 27(6):617–627. https://doi.org/10.1007/bf01337457

Brunchi CE, Bercea M, Morariu S et al (2016) Some properties of xanthan gum in aqueous solutions: effect of temperature and pH. J Polym Res. https://doi.org/10.1007/s10965-016-1015-4

Elkatatny S (2019) Enhancing the rheological properties of water-based drilling fluid using micronized starch. Arab J Sci Eng 44:5433–5442. https://doi.org/10.1007/s13369-019-03720-1

Ma C, Li L, Yang YP, Hao WW, Zhang Q, Lv J (2018) Study on the effect of polymeric rheology modifier on the rheological properties of oil-based drilling fluids. IOP Conf Ser Mater Sci Eng 292:012106. https://doi.org/10.1088/1757-899X/292/1/012106

Fattah S, Blkoor K (2013) The influence of XC-polymer on drilling fluid filter cake properties and formationss damage. J Pet Environ Biotechnol. https://doi.org/10.4172/2157-7463.1000157

Ghasemi N (2018) Investigating created properties of nanoparticles based drilling mud. Heat Mass Trans 54(5):1381–1393. https://doi.org/10.1007/s00231-017-2229-7

Hamed SB, Belhadri M (2009) Rheological properties of biopolymers drilling fluids. J Petrol Sci Eng 67(3–4):84–90. https://doi.org/10.1016/j.petrol.2009.04.001

Hermoso J, Martinez-Boza F, Gallegos C (2014) Influence of viscosity modifier nature and concentration on the viscous flow behaviour of oil-based drilling fluids at high pressure. Appl Clay Sci 87:14–21. https://doi.org/10.1016/j.clay.2013.10.011

HoTeow KCYH, Mohammad AW (2019) Optimization of nanocomposite conductive membrane formulation and operating parameters for electrically-enhanced palm oil milleffluent filtration

using response surface methodology. Process Saf Environ Prot 126:297–308. https://doi.org/10.1016/j.psep.2019.03.019

Ikram R, Mohamed Jan B, Sidek A, Kenanakis G (2021) Utilization of eco-friendly waste generated nanomaterials in water-based drilling fluids; state of the art review. Materials 14(15):4171. https://doi.org/10.3390/ma14154171

Ismail A, Alias A, Sulaiman WRW, Jaafar MZ, Ismail I (2017) Drilling fluid waste management in drilling for oil and gas wells. Chem Eng Trans 56:1351–1356. https://doi.org/10.3303/CET1756226

Ismail AR, Aftab A, Ibupoto ZH, Zolkifile N (2016) The novel approach for the enhancement of rheological properties of water-based drilling fluids by using multi-walled carbon nanotube, nano-silica and glass beads. J Petrol Sci Eng 139:264–275. https://doi.org/10.1016/j.petrol.2016.01.036

Javeri, Saket M, Zishaan W Haindade, Chaitanya BJ (2011) Mitigating loss circulation and differential sticking problems using silicon nanoparticles. SPE/IADC Middle East Drilling Technology Conference and Exhibition

Jiang G, Sun J, He Y, Cui K, Dong T, Yang L, Yang X, Wang X (2022) Novel water-based drilling and completion fluid technology to improve wellbore quality during drilling and protect unconventional reservoirs. Engineering 18:129–142. https://doi.org/10.1016/j.eng.2021.11.014

Karakosta K, Mitropoulos AC, Kyzas GZ (2021) A review in nanopolymers for drilling fluids applications. J Mol Struct 1227:129702. https://doi.org/10.1016/j.molstruc.2020.129702

Kuma M, Das BM, Talukdar P (2020) The effect of salts and haematite on carboxymethyl cellulose–bentonite and partially hydrolyzed polyacrylamide–bentonite muds for an effective drilling in shale formations. J Petrol Explor Prod Technol 10:395–405. https://doi.org/10.1007/s13202-019-0722-x

Lalji SM, Ali SI, Haneef J et al (2022b) Changes in Pakistan crude oil properties contaminated by water-based drilling fluids with varying KCL concentrations. Chem Pap 76:4189–4201. https://doi.org/10.1007/s11696-022-02154-8

Lalji SM, Ali SI, Ahmed R et al (2022a) Influence of graphene oxide on salt-polymer mud rheology and Pakistan shale swelling inhibition behavior. Arab J Geosci. https://doi.org/10.1007/s12517-022-09800-1

Lalji SM, Khan MA, Haneef J et al (2023) Nano-particles adapted drilling fluids for the swelling inhibition for the Northern region clay formation of Pakistan. Appl Nanosci. https://doi.org/10.1007/s13204-021-01825-4

Li M-C, Qinglin Wu, Song K, Qing Y, Yiqiang Wu (2015) Cellulose nanoparticles as modifiers for rheology and fluid loss in bentonite water-based fluids. ACS Appl Mater Interfaces 7(8):5006–5016. https://doi.org/10.1021/acsami.5b00498

Mao H, Qiu Z, Shen Z, Huang W (2015) Hydrophobic associated polymer based silica nanoparticles composite with core–shell structure as a filtrate reducer for drilling fluid at utra-high temperature. J Petrol Sci Eng 129:1–14. https://doi.org/10.1016/j.petrol.2015.03.003

Martin C, Babaie M, Nourian A, Nasr GG (2023) Designing smart drilling fluids using modified nano silica to improve drilling operations in geothermal wells. Geothermics 107:102600. https://doi.org/10.1016/j.geothermics.2022.102600

Medved I, Gaurina-Međimurec N, Mavar KN, Mijić P (2022) Waste mandarin peel as an eco-friendly water-based drilling fluid additive. Energies 15(7):2591. https://doi.org/10.3390/en15072591

Minakov AV, Mikhienkova EI, Zhigarev VA, Neverov AL, Rudyak VY (2018) A study of the influence of nanoparticles on the properties of drilling fluids. Colloid J 80(4):418–426

Khodja M, Khodja-Saber M, Canselier JP, Cohaut N, Bergaya F (2010) Drilling Fluid Technology: Performances and Environmental Considerations. In Products and Services, edited by Fuerstner Igor, Ch. 13. Rijeka: IntechOpen

Ng ZJ et al (2020) Synthesis of silica-coated iron oxide nanoparticles: effect of particle sizes and silica coating. Int J Nanoelectron Mater 13(3):565–576

Nmegbu C (2014) Laboratory investigation of rivers state clay samples for drilling mud preparation. J Eng Res Appl 4(6):70–76

Özkan A, Turan S, Özkan V (2020) Experimental investigation of the effects on rheological and filtration properties of water-based drilling mud of fly ash addition with different particle size and concentration. Erzincan Univ J Sci Technol 13(3):1217–1227

Rafieefar A, Sharif F, Hashemi A, Bazargan AM (2021) Rheological behavior and filtration of water-based drilling fluids containing graphene oxide: experimental measurement, mechanistic understanding, and modeling. ACS Omega 6(44):29905–29920. https://doi.org/10.1021/acsomega.1c04398

Rezaei A, Nooripoor V, Shahbazi K (2020) Applicability of Fe_3O_4 nanoparticles for improving rheological and filtration properties of bentonite-water drilling fluids in the presence of sodium, calcium, and magnesium chlorides. J Petrol Explor Prod Technol 10:2453–2464. https://doi.org/10.1007/s13202-020-00920-6

Sajjadian M, Sajjadian VA, Rashidi A (2020) Experimental evaluation of nanomaterials to improve drilling fluid properties of water-based muds HP/HT applications. J Petrol Sci Eng 190:107006. https://doi.org/10.1016/j.petrol.2020.107006

Sangwai, Jitendra S (2020) Nanotechnology for energy and environmental engineering: Springer

Tahr Z, Ali JA, Mohammed AS (2023) Sustainable aspects behind nano-biodegradable drilling fluids: a critical review. Geoenergy Sci Eng 222:211443. https://doi.org/10.1016/j.geoen.2023.211443

Ullah R, Deb BK, Mollah MYA (2014) Synthesis and characterization of silica coated iron-oxide composites of different ratios. Int J Compos Mater 4(2):135–145. https://doi.org/10.5923/j.cmaterials.20140402.13

Villa S, Riani P, Locardi F, Canepa F (2016) Functionalization of Fe_3O_4 NPs by silanization: use of amine (APTES) and thiol (MPTMS) silanes and their physical characterization. Materials 9(10):826

Vryzas Z, Kelessidis VC (2017) Nano-based drilling fluids: a review. Energies. https://doi.org/10.3390/en10040540

Vryzas Z, Mahmoud O, Nasr-El-Din H, Zaspalis V, Kelessidis VC (2016) Incorporation of Fe_3O_4 nanoparticles as drilling fluid additives for improved drilling operations. International Conference on Offshore Mechanics and Arctic Engineering

Wang T, Ni M, Luo Z et al (2012) Viscosity and aggregation structure of nanocolloidal dispersions. Chin Sci Bull 57:3644–3651. https://doi.org/10.1007/s11434-012-5150-y

Xie B, Ting Li, Zhang Y, Liu C (2018) Rheological properties of bentonite-free water-based drilling fluids with novel polymer viscosifier. J Petrol Sci Eng 164:302–310. https://doi.org/10.1016/j.petrol.2018.01.074

Yalman E, Federer-Kovacs G, Depci T, Khalaf HA, Aylikci V, Aydin MG (2022) Development of novel inhibitive water-based drilling muds for oil and gas field applications. J Petrol Sci Eng 210:109907. https://doi.org/10.1016/j.petrol.2021.109907

Zhang J, Chen G, Yang NW (2012) Development of a new drilling fluid additive from lignosulfonate. Adv Mater Res

Zhao X, Li D, Zhu H, Ma J, An Y (2022) Advanced developments in environmentally friendly lubricants for water-based drilling fluid: a review. RSC Adv 12(35):22853–22868. https://doi.org/10.1039/D2RA03888A